Chemistry–A European Journal
Research Article
doi.org/10.1002/chem.202402365
Chemistry Europe
European Chemical Societies Publishing

www.chemeurj.org

Self-Assembly of Chemically Programmed Amphiphiles into Aqueous Nanotubes with a Lipophilic Lumen

Fátima Aparicio,[a, d] Irene Sancho-Casado,[a] Paula B. Chamorro,[a] Marina González-Sánchez,[a] Silvia Pujals,[b] Victor Vega-Mayoral,[c] and David González-Rodríguez*[a, d]

The creation of complex hollow nanostructures with precise control over size and shape represents a great challenge in supramolecular soft materials. Here, we have further developed a bioinspired methodology for the formation of aqueous nanotubes of well-defined dimensions and pore coating through the self-assembly of amphiphiles that are chemically programmed with complementary nucleobases. These nanotubes are endowed with a hydrophobic lumen, whose diameter can be expanded as a function of the monomer length, in which apolar dyes can be efficiently encapsulated.

Introduction

In nature, confined cavities provide recognition sites for host-guest interactions. These specific nanospaces are important, for example, for the binding of substrates to enzymes to execute catalytic reactions.[1] Inspired by these biological systems, much effort has been devoted by supramolecular chemists to the design of artificial nanoconfined spaces in self-assemblies, so as to target applications in molecular recognition, sensing, and catalysis.[2] The most common strategy historically employed considers the formation of hydrophobic environments in aqueous solution through the organization of amphiphilic molecules in, for instance, micellar architectures.[3] All the hydrophobic groups that don't show an affinity for the solvent tend to group within the assembly, while the hydrophilic groups are instead disposed towards the external aqueous medium.

However, it is still challenging to create complex hollow nanostructures from simple amphiphilic molecules with precise (*i.e.* sub-nanometer) control over size and shape.[4] Several advantages would be acquired if such goal succeeds: 1) the use of small molecule building blocks allows to make multiple structural modifications with minimum synthetic cost; 2) the soft, reversible nature of the assembled structures may enable controlled guest release upon application of a stimulus; 3) a highly precise control of cavity dimensions may open the door to selectivity upon substrate uptake. Even though many recent investigations have focused on the design and development of self-assembled nanotubes through the stacking of discrete supramolecular cycles formed by small molecules,[4a,d,f,5] very little attention has been put onto tailoring their external and internal interfaces with chemical groups of different nature, so as to target applications as selective aqueous nanocontainers.[6]

In this context, we recently developed a versatile and unconventional approach for the generation of self-assembled nanotubes that exploited, in a cooperative and hierarchical manner, H-bonding between complementary DNA bases and stacking interactions between macrocyclic rings.[7] In order to take this strategy to aqueous environments, amphiphilic dinucleobase molecules are programmed with directional and complementary Watson-Crick H-bonds, which must be shielded from the competing water within a lipophilic shell to associate in rectangular tetrameric assemblies.[8] Upon stacking of these cyclic sections, micelle-like nanotubes with a hydrophobic lumen of controlled dimensions and chemical coating are generated.[8]

Here, we further prove the success of this strategy with a monomer comprising an amphiphilic biphenyl central block in between guanine (G) and cytosine (C) bases (**GC2**; Figure 1) that generates larger water-soluble nanotubes, having a diameter of about 4 nm. Moreover, these nanotubes are endowed with a confined nanospace that is able to encapsulate molecules that are complementary in size and shape, and that show a higher affinity for the lipophilic pore coating than for the external aqueous media. Our new **GC2** design is intended to adjust and improve some aspects with respect to the self-assembly of **GC1**. Firstly, we want to prove that nanotube pore diameter can be fine-tuned as a function of the length of the spacer connecting the bases, which might lead to higher guest loadings or to the encapsulation of larger guests. Secondly, an extended π-conjugated central block should enhance hydrophobic inter-

[a] F. Aparicio, I. Sancho-Casado, P. B. Chamorro, M. González-Sánchez, D. González-Rodríguez
Organic Chemistry Department, Universidad Autónoma de Madrid, 28049, Madrid, Spain
E-mail: david.gonzalez.rodriguez@uam.es

[b] S. Pujals
Institute of Advanced Chemistry of Catalonia, 08034, Barcelona, Spain

[c] V. Vega-Mayoral
Madrid Institute for Advanced Studies, IMDEA Nanociencia, 28049, Madrid, Spain

[d] F. Aparicio, D. González-Rodríguez
Institute for Advanced Research in Chemical Sciences (IAdChem), Universidad Autónoma de Madrid, 28049, Madrid, Spain

Supporting information for this article is available on the WWW under https://doi.org/10.1002/chem.202402365.

Research Article
doi.org/10.1002/chem.202402365
Chemistry Europe
European Chemical Societies Publishing

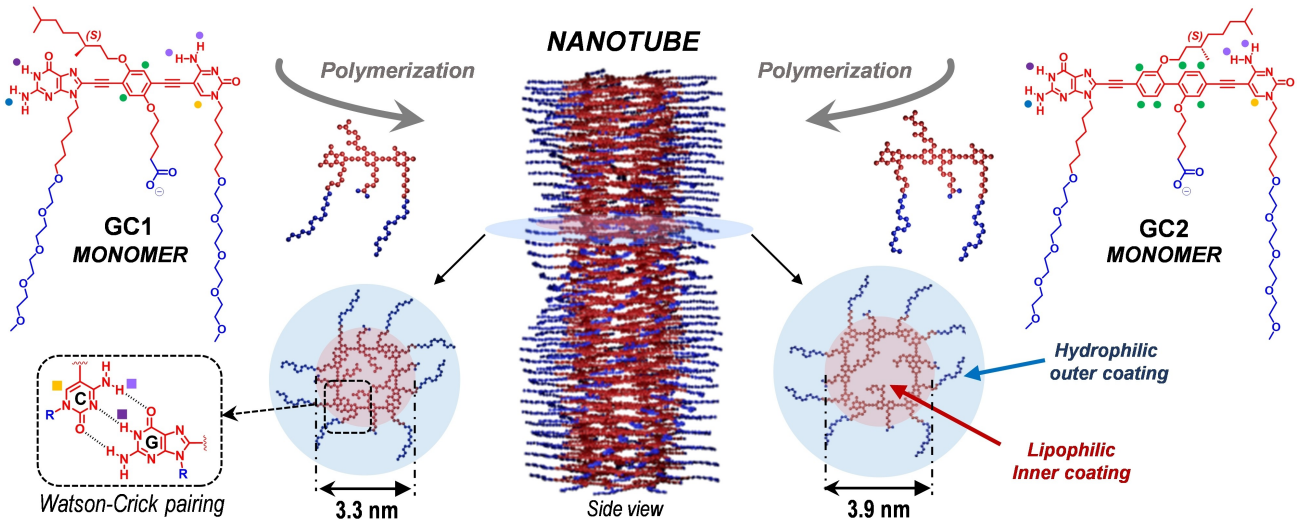

Figure 1. Structure of the amphiphilic **GC1** and **GC2** dinucleobases and schematic representation of their self-assembly into nanotubes. Hydrophobic and hydrophilic parts are shown in red and blue, respectively. Note that only one of the 2 possible **GC1** and **GC2** regioisomers is represented (see the S.I. for more information).

actions and thus result in stronger assemblies. This was a drawback in the case of **GC1** when trying to visualize the tubular structures by fluorescence microscopy, due to strong contamination by the intense residual monomer emission because of incomplete self-assembly.

Results and Discussion

The synthesis of compounds **GC1** and **GC2**, having respectively phenyl and biphenyl central blocks, required the preparation and coupling of 3 main units, as detailed in earlier work for **GC1**[8] and at the S. I. of this work for **GC2** (Section S0). On one hand, G and C derivatives were equipped with alkyl chains that start with a hydrophobic alkane segment, with the aim to protect Watson-Crick pairing from the H-bond-competing environment, and finish with hydrophilic ethylene glycol units, so as to impart solubility in water to the ensemble. On the other, the central phenyl/biphenyl block was endowed with a hydrophilic carboxylate group on one side, and a chiral lipophilic chain on the other, which serves to try to bias the helical sense in the final columnar stacks. The choice of this new 2,2′-dialkoxybiphenyl central block was made attending to different reasons: i) it is a rather planar biphenyl derivative with a fixed conformation where the alkoxy groups adopt an *"anti"* orientation to avoid electronic repulsion, thus guaranteeing that the lipophilic and hydrophilic chains will point to opposite sides of the monomer axis, as it happens in **GC1**; ii) it affords a moderately higher monomer length, that would be translated into nanotube diameters of just about 0.5–1.0 nm wider; iii) it presents an extended hydrophobic π-surface, which should enhance aggregation strength in water with respect to **GC1**; and finally iv) it supplies an additional candidate to test the reproducibility and enlarge the scope of our supramolecular approach.

Diluted solutions of **GC1** and **GC2** in water reveal the same spectroscopic features that can be ascribed to supramolecular aggregation (Figure 2): the ^{1}H NMR signals broaden and vanish, red-shifted absorption and emission features appear, emission intensity decreases, and a Cotton effect emerges in the CD spectrum, which has a negative sign for both monomers. However, such CD response, attributed to a helical aggregate organization, only emerged in aged samples, so we performed a more detailed investigation to study their evolution as a function of time.

Whereas monomer **GC1** required a few hours to reach the maximum CD response at room temperature, the timescale for **GC2** was extended to several days (Figure S9). On the contrary, absorption experiments revealed an instantaneous aggregation process (see below), and no additional changes were observed after hours or days. We attribute this effect to the fact that the self-assembled structures may keep increasing internal chiral order with time even after they are fully formed, so the measured timescales indicate very slow helical organization processes, especially for **GC2**. This could be due to changes in the chiral chromophore arrangement influenced by a very subtle communication between the *S*-chiral lipophilic chains at the central blocks. In addition to the different conformations that this chain can adopt, the phenyl/biphenyl central blocks can rotate so as to place this chiral group within or out of the pore, though it is expected that most of these alkyl chains will concentrate, with time, inside the tube's lumen, due to hydrophobic repulsion. Furthermore, compounds **GC1** and **GC2** are actually composed of a 1:1 mixture of regioisomers (see S.I.) that have this lipophilic chain in *meta*-position to either the ethynylene group connecting to the C base or the one linking to the G base. The dynamic reorganization of these regioisomers along the polymer structure, so as to reach the most stable helical arrangement, may be another reason for the slow growth of the CD signal in water. It is in any case clear that

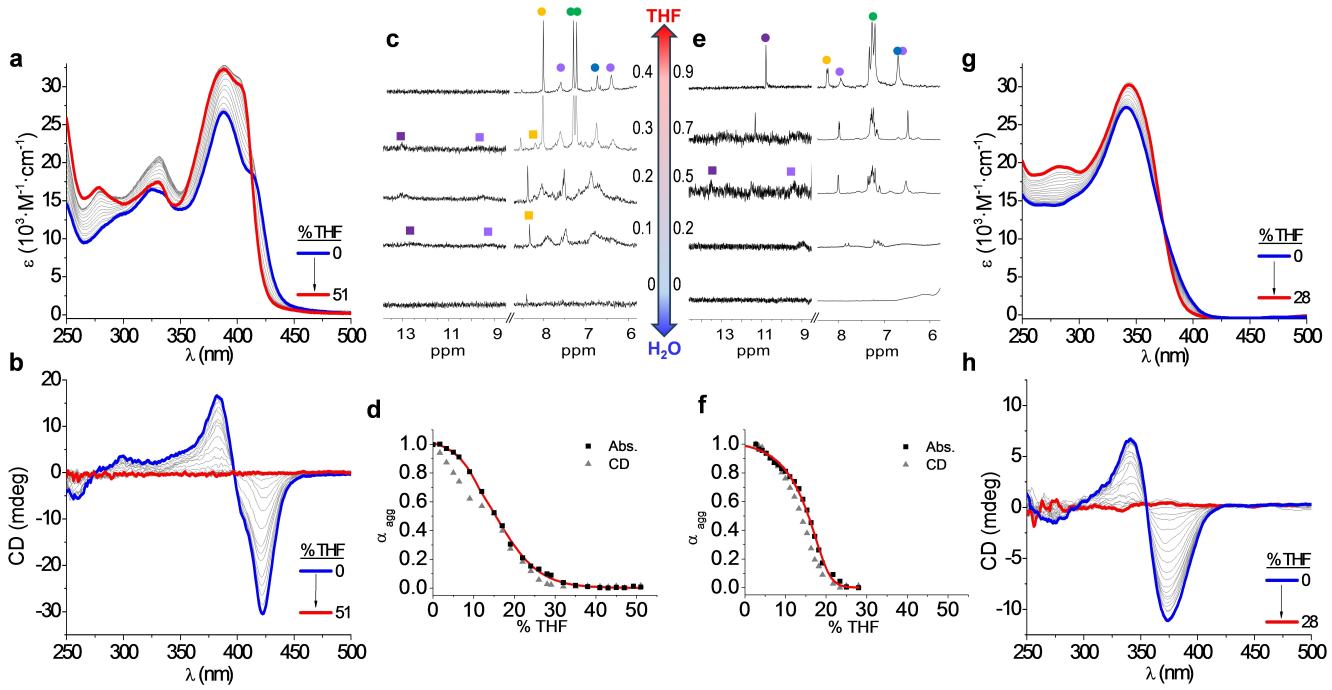

Figure 2. Solvent-dependent experiments monitored by (a, g) UV-Vis, (c, e) ^{1}H NMR and (b, h) CD of (a, b, c) **GC1** and (e, g, h) **GC2** in H_2O/THF mixtures at 5.0×10^{-5} M (UV-vis, CD) or 1.0×10^{-3} M (NMR) and 298 K. Circles and squares in (c, e) indicate protons in the monomer and aggregated species, as designated in Figure 1. The volume fraction of THF-d_8 in H_2O is indicated at the side of each spectrum. The top spectrum in (e) contains a tiny amount of DMSO-D_6 to fully dissociate **GC2**. (d, f) Depolymerization curves acquired from the UV-Vis and CD data for (d) **GC1** and (f) **GC2**, and fitting to the nucleation-elongation model (red line).

these conformational rearrangements and/or monomer exchange processes required to maximize the chiral response are considerably slower for **GC2** than for **GC1**, which suggests a higher kinetic stability of the aggregates of **GC2**.

The stable aggregates formed in water can be denatured by increasing the volume fraction of THF in this solvent (V_{THF}), so that above $V_{THF} > 0.25$ at a 5.0×10^{-5} M concentration, the monomer state is reached, which displays well-defined ^{1}H NMR signals, high intensity emission at 422 nm and null CD signal (Figure 2). The depolymerization process upon increasing V_{THF} could be monitored by UV–Vis and fitted to the corresponding nucleation–elongation model,[9] which allowed the determination of the Gibbs free energy gain upon monomer addition (ΔG^0), as well as the degree of cooperativity (σ) (Table 1). By means of this quantitative thermodynamic analysis, both substances led to very similar degrees of cooperativity ($\sigma = 0.44$ for **GC1**, 0.31 for **GC2**). The aggregation transition can also be monitored by ^{1}H NMR as a function of the volume fraction of THF-d_8 at higher concentrations (i.e. $> 10^{-4}$ M; Figure 2c,e). Both **GC1** and **GC2** display very broad NMR signals in aqueous samples, which is consistent with the formation of polymeric species, but as the content of THF is increased the signals become better defined until the monomer state is reached. Interestingly, evidence for G:C Watson-Crick pairing can be obtained in both cases at intermediate THF:H_2O compositions, as noted in the characteristic G-amide and C-amine H-bonded proton signals detected above 9 ppm (marked with squares in Figures 2c, e).

The supramolecular polymers in water of **GC2** are, nonetheless, very resistant to temperature variations, and no change in

Table 1. Thermodynamic parameters calculated for **GC1** and **GC2** upon (a) depolymerization by increasing V_{THF} at 5.0×10^{-5} M by UV-Vis spectroscopy and (b) polymerization by decreasing temperature at $V_{THF} = 15\%$ and 1.0×10^{-5} M by fluorescence spectroscopy.

		σ [a]	*m* (KJ/mol)[b]	Δ*G* (KJ/mol)[c]	K_n (M^{-1})[d]	K_e (M^{-1})[e]	ΔH^0 (KJ/mol)[f]	ΔS^0 (J/mol·K)[g]	ΔH_n^0 (KJ/mol)[h]	T_e (K) [i]
a	**GC1**	0.44 ± 0.04	49.6 ± 1.4	−36.1 ± 0.2	–	–	–	–	–	–
	GC2	0.31 ± 0.10	46.4 ± 9.0	−38.1 ± 1.9	–	–	–	–	–	–
b	**GC1**	1.2×10^{-2}	–	–	2.6×10^3	2.2×10^5	−68.5 ± 6.8	−127.6 ± 23.6	−11.0 ± 1.0	303.4 ± 0.3
	GC2	1.3×10^{-3}	–	–	3.0×10^2	2.3×10^5	−48.0 ± 1.6	−58.2 ± 5.2	−16.4 ± 0.8	311.6 ± 2.1

[a] Degree of cooperativity, [b] m Parameter and [c] Gibbs free energy of the depolymerization process observed by increasing V_{THF}. [d] Nucleation and [e] elongation constants, elongation [f] enthalpy and [g] entropy, nucleation [h] enthalpy and [i] elongation temperature of the polymerization process calculated upon cooling.

absorption could be appreciated within the 273–333 K range (Figure S10). However, important CD changes were noted upon heating. As shown in Figure S10, the stable and clear bisignated signal acquired at room temperature changed in intensity and sign with temperature and time, a phenomenon that was also observed for **GC1** in previous work,[8b] and that we attribute to a reorganization of the helical aggregates due to the dehydration of the ethylene oxide chains above a critical temperature, similar to the case of lower critical solution temperature (LCST).[10] Contrarily to classical LCST behavior, we do not see any cloud point and the solubility of the solution remains unaltered. The recovery of the original CD spectrum upon cooling back to room temperature was not immediate, but required again several days. In order to avoid this dehydration events and record the whole supramolecular polymerization from the monomer, the concentration of the sample was lowered to 1.0×10^{-5} M and 15% THF was added (Figure 3). Although no CD signal was observed under these conditions, cooling experiments performed by UV–Vis and fluorescence spectroscopies enabled us to analyze the complete polymerization process (Figure 3). In UV–vis, a single absorption band centered at 343 nm was detected, accompanied by an emission band at 432 nm. Even though only a small decrease in intensity was detected in UV and fluorescence with the decrease of temperature, together with a slight red-shift of the emission band, cooling experiments performed by these techniques revealed non-sigmoidal curves that could be fitted to a nucleation-elongation model,[11] which afforded the elongation enthalpy ($\Delta H°$) and entropy ($\Delta S_e°$), the nucleation enthalpy ($\Delta H_n°$), the nucleation (K_n) and elongation (K_e) equilibrium constants, as well as the cooperativity factor (σ) of the polymerization process (Table 1). A first comparison between the cooling curves of **GC1** and **GC2** (Figure 3e) reveals a higher elongation temperature for the latter ($T_e = 303$ K for **GC1** and 312 K for **GC2**), which confirms the predicted higher thermal stability of the polymers containing the larger biphenyl core. Besides, the corresponding fittings resulted now in a higher degree of cooperativity for **GC2** ($\sigma = 1.3\times10^{-3}$) than for **GC1** ($\sigma = 1.2\times10^{-2}$), which stems from a smaller nucleation constant.

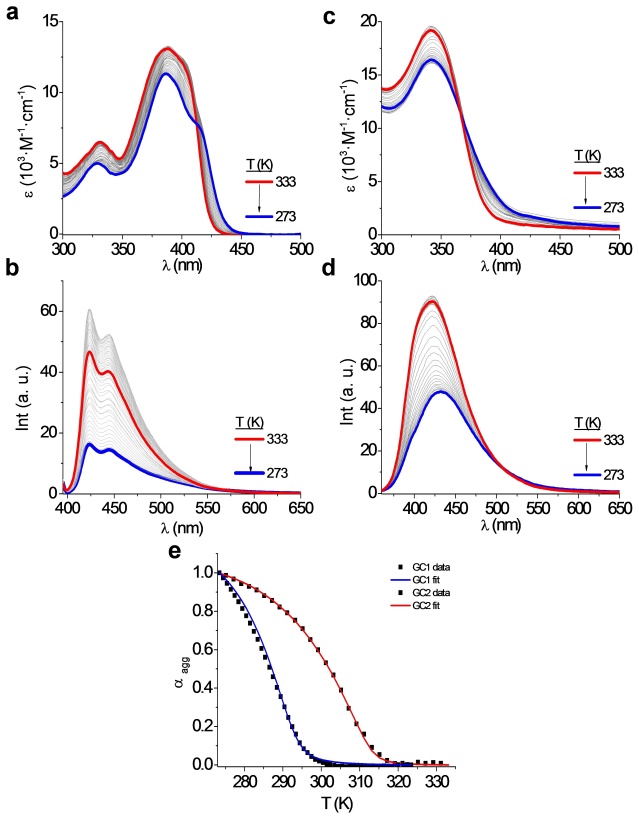

Figure 3. Temperature-dependent (a, c) UV–Vis and (b, d) emission experiments of compound (a, b) **GC1** and (c, d) **GC2** ($\lambda_{exc} = 390$ and 348 nm, respectively) in H_2O/THF 85:15 at 1.0×10^{-5} M ($l = 1$ cm). (e) Corresponding curves from emission data for both compounds at a fixed wavelength (422 nm) and fitting to the nucleation-elongation model (blue and red lines).

We next investigated the morphology of the aggregates formed by **GC2** by AFM and TEM microscopies, to compare with the results previously obtained for **GC1**, as displayed in Figures 4 and S11–13. In both techniques and for both compounds, the presence of unidimensional objects was observed. Although in some cases individual longitudinal polymers were spotted, it was quite frequent to observe heavily bundled fibers, both in AFM and TEM. The last technique revealed a high contrast (darker) profile at the walls of these fibers and a low contrast (lighter) section in the middle, which is consistent with the formation of hollow tubular assemblies. Height dimensions measured by AFM (~2.0–3.5 nm for **GC1** and ~3.5–4.5 nm for **GC2**; Figure 4d) and width dimensions obtained by the analysis of multiple TEM images (~5.8 ± 0.7 nm for **GC1** and 7.6 ± 1.1 nm for **GC2**; Figure 4e) match rather well with the section expected from our models (Figures 4f and S14) and confirm the larger diameter of the aggregates formed by the novel biphenyl-containing monomer. The slightly smaller diameter measured by AFM is attributed to compression effects caused by both the surface-assembly interactions and the force applied by the tip.[12]

An indirect approach to test the hydrophobicity of the cavity created in the nanotube, according to our design, consists in proving the selective encapsulation of apolar substances, insoluble in water, into the tube's pore. For that purpose, mixtures with the well-known fluorescent hydrophobic dye Nile Red (**NR**) were investigated (Figures 5 and S16). Compound **GC2** and **NR** (0.5 eqs.) were mixed in water and measured by UV–Vis and emission spectroscopies (selectively exciting **NR** at 588 nm or **GC2** at 348 nm). The results were compared with those of isolated **GC2** or **NR** control samples under identical experimental conditions within a concentration window of 10^{-4} to 10^{-5} M (see Figures S16 and S19). Dye extraction was confirmed by an increase in the absorbance (Figure 5c) and emission (Figure 5e) of the dye when mixed with the **GC2** nanotubes. Moreover, a blue-shifted **NR** emission, from ca. 655 nm to 630 nm (see Figures 5e and S16 and S19), was noted in the mixtures, which is characteristic of this fluorescent probe when surrounded by apolar environments.[13] These observations were ascribed to the solubilization of the dye due to its encapsulation within the hydrophobic pocket created within the nanotubes. Experiments performed under

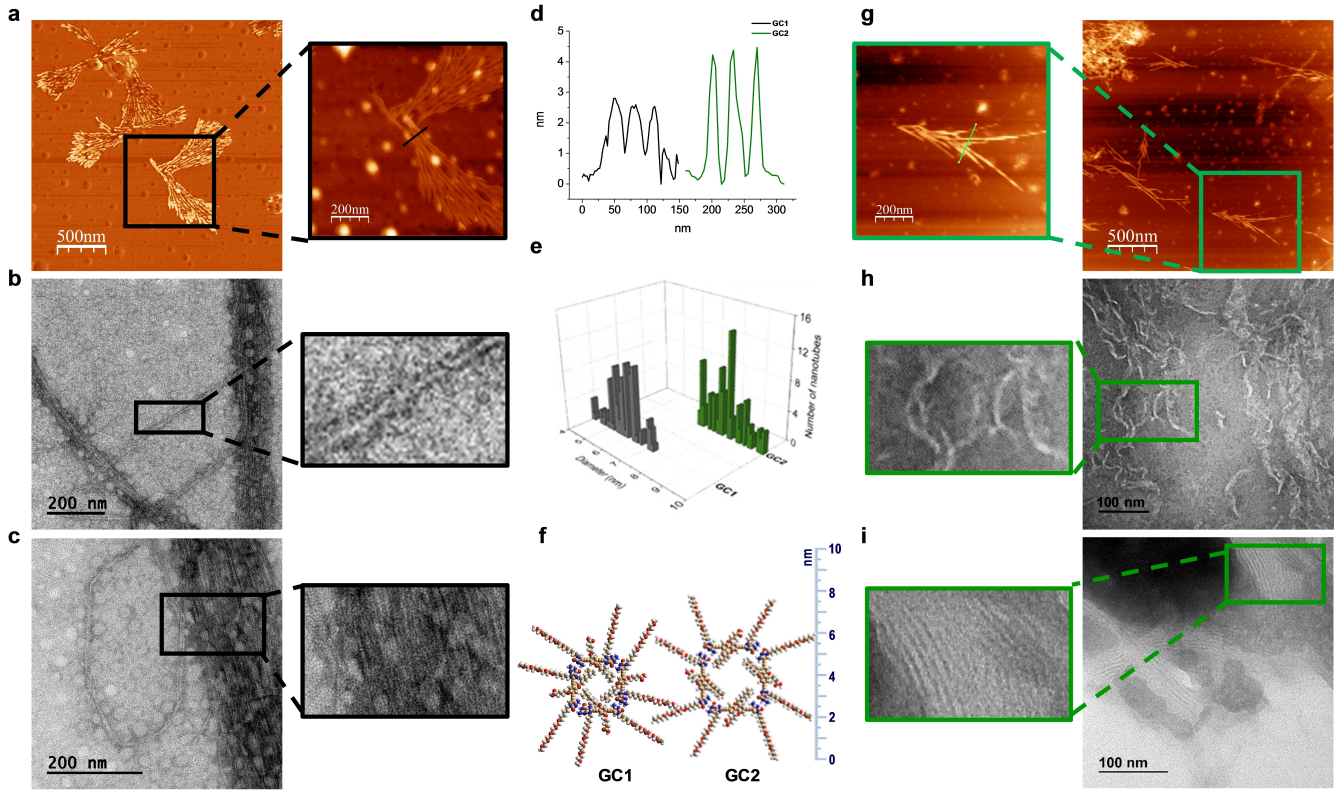

Figure 4. Microscopy measurements of (a, b, c) **GC1** and (g, h, i) **GC2** deposited by drop-casting from 5.0×10^{-7} M H_2O solutions onto (a) HOPG and (g) mica, and imaged by AFM, or (b, c, i) C-Formvar Cu grids and (h) C-Formvar Ni grids treated by glow discharge and stained with uranyl acetate, and imaged by TEM. (d) Nanotube height profiles measured by AFM. (e) Diameter distribution measured by TEM. (f) CPK Models and relative dimensions of the **GC1**/**GC2** nanotube sections.

identical conditions for **GC1** nanotubes led to very similar results, as reproduced in Figures 5b, d and S15, S18.

Interestingly, when **GC1**/**GC2** was selectively excited in the 350–390 nm region in the mixtures, an emission quenching, accompanied by the appearance of the **NR** emission at 628 nm, was noted (Figure S15c and S16d), despite **NR** alone did not show emission when excited at the same wavelength, which is due primarily to its lack of solubility in water, but also to a low absorbance in this spectral region. This is consistent with an energy transfer process from **GC1**/**GC2** to the **NR** probe, which was confirmed by excitation experiments (Figure S16c), and suggests that these two molecules are in close proximity. We additionally performed time-resolved fluorescence measurements to evaluate the emission lifetime changes experienced by **GC1**/**GC2** and by **NR** upon guest encapsulation within the nanotubes in water (Figure S20–S21). On one hand, nanotube emission decay dynamics accelerates when **NR** is extracted, which is an additional sign of energy transfer. For the assemblies of **GC1** and **GC2** in water the average lifetimes are reduced from $\tau_D = 0.62$ to $\tau_{DA} = 0.30$ ns, in the first case, and from $\tau_D = 0.09$ to $\tau_{DA} = 0.07$ ns, in the second, upon **NR** encapsulation, where τ_{DA} and τ_D are the lifetimes of the donor molecule in the presence and absence of the acceptor. On the other, **NR** decay dynamics is also modified substantially when embedded in the nanotubes, exhibiting an average fluorescence lifetime of $\tau_A = 0.15$ ns and $\tau_A = 0.53$ ns, in **GC1** and **GC2** assemblies, respectively, in comparison to the $\tau_A = 3.39$ ns recorded when solubilized in ethanol. The efficiency (E) of the energy transfer can be then calculated using the expression $E = (1 - \tau_{DA}/\tau_D)\times100$, leading to values of 52% and 22% for **GC1** and **GC2** respectively.

The encapsulation efficiency, that is, the maximum amount of dye extracted by the **GC1**/**GC2** nanotubes, was calculated through titration experiments with increasing amount of **NR**. Our results (Figure S22) indicate that saturation occurs around 0.2–0.4 equivalents of added dye per **GC1**/**GC2** monomer, suggesting that **NR** molecules are nested in the lipophilic pores in between cyclic tetramers. However, no measurable differences in dye extraction capability were noted between the nanotubes of **GC1** or **GC2**. Moreover, control TEM images of drop-casted **NR** and **GC2** mixtures in water showed again unidimensional objects that indicated that the morphology of **GC2** assembles was maintained and not disrupted due to the presence of the dye molecules (Figure S25). In addition, we tested other dyes that are insoluble in water and that absorb and emit at longer wavelengths than our **GC1**/**GC2** molecules, which include a BODIPY derivative (**BPY**) and Disperse Blue 14 (**DB**). The results obtained in absorption and emission measurements, as displayed in Figures S23 and S24 respectively, were very similar to those recorded for **NR**.

Next, we evaluated whether the aggregates could be visualized by fluorescence microscopy with the help of the

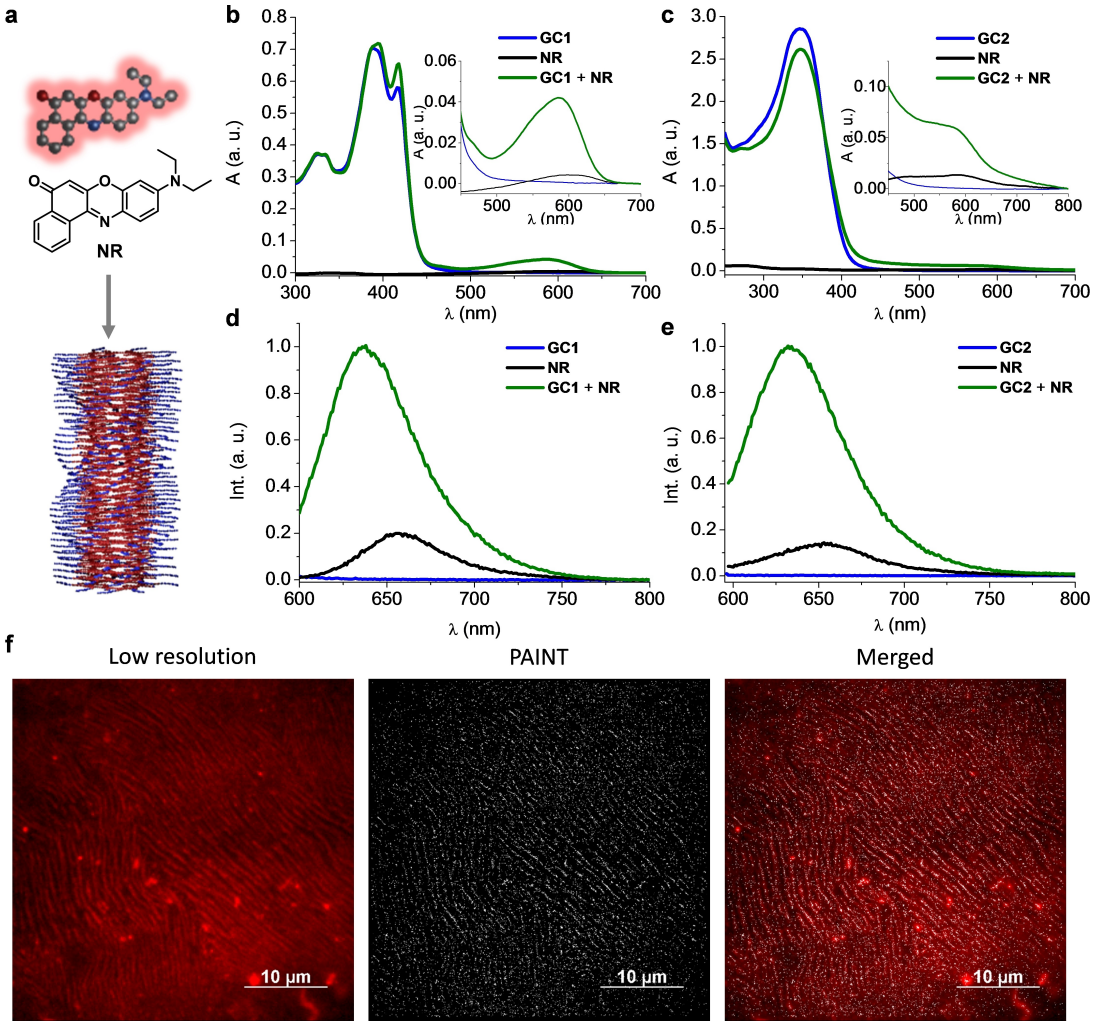

Figure 5. (a) Chemical structure of Nile Red (**NR**) and schematic representation of its encapsulation inside nanotubes. (b, c) Absorption, (d,e) emission (λ_{exc} = 588 nm) spectra of (b,d) **GC1** and (c,e) **GC2** (in blue), **NR** (in black), and their mixture (in green) in Milli-Q water ([**GC1**] = 2.0×10^{-4} M and [**NR**] = 2.0×10^{-5} M, [**GC2**] = 1.0×10^{-4} M and [**NR**] = 5.0×10^{-5} M; *l* = 1 mm for **GC1** and *l* = 1 cm for **GC2**). Inset in b,c shows a zoom of the dye absorption area. (f) Low resolution (left), PAINT (middle) and corresponding merged (right) images of the **GC2** nanotubes (5.0×10^{-7} M) in the presence of **NR** molecules (1.25×10^{-7} M) in Milli-Q water.

emission coming from the encapsulated **NR** molecules in the nanotube. For that purpose, we chose the point accumulation for imaging in nanoscale topography (PAINT)[14] to picture our nanotubes. PAINT is based on the reversible photoactivation of fluorescent probes. Through this approach, the dye emission is photocontrolled and the fluorophores can be switched on and off with laser illumination, enabling molecular localization with high accuracy and the construction of a super resolution map of the object of interest. These experiments were not successful for **GC1**, because the nanotubes were insufficiently stable, and the strong residual monomer emission contaminated the images. However, the higher stability of the supramolecular nanotubes formed by **GC2** enabled us to acquire images through the PAINT technique in a reliable and reproducible manner.

Thus, compound **GC2** (5.0×10^{-7} M) and **NR** (1.25×10^{-7} M) were mixed in water and deposited on glass coverslips suitable for the PAINT equipment (for experimental protocols, see S.I.). The photocontrolled emission of **NR** molecules obtained by the selective irradiation of the sample at 561 nm, led to PAINT images (Figures 5f and S26) in which multiple clear nanofilaments could be observed. The alignment of **NR** emission points in the form of lines in the image corroborated the presence of dye molecules within the hydrophobic lumen of **GC2** nanotubes. These lines could be easily identified in the corresponding low resolution image of the same area (prior to photocontrolled emission of **NR**) of the sample in which multiple complete nanotubes could be visualized. Moreover, control experiments of **GC2** nanotubes (5.0×10^{-7} M) in the absence of **NR** and of **NR** alone (1.25×10^{-7} M), both in identical experimental conditions to the previous measurements, led, in contrast, to very poor emission in the first case (Figure S27) (note that, by using a 561 nm laser, only **NR** molecules are excited) and to emission coming from very different morphologies in the other (Figure S28). In none of the control experi-

ments, emission points specifically organized in longitudinal orientations was observed.

Conclusions

In summary, we have demonstrated that the combination of hydrophobic forces and directional H-bonding interactions, encoded in the monomer structure, can provide tubular amphiphilic assemblies with a precisely defined shape, of rectangular section, size, which was extended to over 4 nm in diameter, and with a lipophilic pore coating. The use of apolar dye probes, like **NR**, in spectroscopic and fluorescence microscopy experiments corroborated the formation of nanoconfined hydrophobic cavities within the nanotubes, in which these apolar guests are nested.

Supporting Information Summary

Additional supporting information can be found online in the Supporting Information section at the end of this article.

Acknowledgements

This work was supported by MCIN (PID2020-116921GB-I00, TED2021-132602B-I00) and AEI (PID2020-116112RJ-I00). F.A. is grateful to MCIN and Next Generation EU funding for a "Ramon-y-Cajal" fellowship (RyC-2021-031538-I). P. B. C. is grateful to the Comunidad de Madrid for the PEJ-2017-AI/IND-6246 contract. V V.-M. acknowledges grants TED2021-131906A-100, PID2021-128313OB-I00 and CNS2022-136191, funded by the Spanish Ministry of Science, Innovation and Universities (10.13039/501100011033), as well as support from the Regional Government of Madrid (2019-T2/IND-12737).

Conflict of Interests

The authors declare no conflict of interest.

Data Availability Statement

The data that support the findings of this study are available from the corresponding author upon reasonable request.

Keywords: Amphiphiles · Encapsulation · Nanotubes · Self-assembly · Supramolecular

[1] a) D. Ringe, G. A. Petsko, *Science* **2008**, *320*, 1428–1429; b) P. K. Agarwal, *Microb. Cell Fact.* **2006**, *5*, 2.
[2] a) S. Aggarwal, S. Ikram, *Biotechnol Bioeng.* **2023**, *120*, 352–398; b) A. Harada, Y. Takashima, A. Hashidzume, H. Yamaguchi, *Bull. Chem. Soc. Jpn.* **2021**, *94*, 2381–2389; c) M. J. Wiester, P. A. Ulmann, C. A. Mirkin, *Angew. Chem. Int. Ed.* **2011**, *50*, 114–137; d) Q. Wang, G. Yang, Y. Fu, N. Li, D. Hao, S. Ma, *ChemNanoMat* **2022**, *8*, e202100396; e) D. M. Kaphan, M. D. Levin, R. G. Bergman, K. N. Raymond, F. D. Toste, *Science* **2015**, *350*, 1235–1238; f) A. Corma, *Catal. Rev.* **2004**, *46*, 369–417.
[3] a) M. Akamatsu, *J. Oleo Sci.* **2023**, *72*, 105–116; b) R. W. Jadhav, D. N. Nadimetla, V. K. Gawade, L. A. Jones, S. V. Bhosale, *Chem. Rec.* **2023**, *23*, e202200180; c) G.-D. Fu, G. L. Li, K. G. Neoh, E. T. Kang, *Prog. Polym. Sci.* **2011**, *36*, 127–167.
[4] a) P. B. Chamorro, F. Aparicio, *Chem. Commun.* **2021**, *57*, 12712–12724; b) R. Chapman, M. Danial, M. L. Koh, K. A. Jolliffe, S. Perrier, *Chem. Soc. Rev.* **2012**, *41*, 6023–6041; c) J. Montenegro, M. R. Ghadiri, J. R. Granja, *Acc. Chem. Res.* **2013**, *46*, 2955–2965; d) A. Nitti, A. Pacini, D. Pasini, *Nanomaterials* **2017**, *7*, 167; e) R. L. Beingessner, Y. Fan, H. Fenniri, *RSC Adv.* **2016**, *6*, 75820–75838; f) B. Adhikari, X. Lin, M. Yamauchi, H. Ouchi, K. Aratsu, S. Yagai, *Chem. Commun.* **2017**, *53*, 9663–9683; g) C.-Z. Liu, M. Yan, H. Wang, D.-W. Zhang, Z.-T. Li, *ACS Omega* **2018**, *3*, 5165–5176.
[5] T. Shimizu, *Bull. Chem. Soc. Jpn.* **2018**, *91*, 623–668.
[6] a) S. Song, Y. Chen, Z. Yan, H. Fenniri, T. J. Webster, *Int. J. Nanomedicine* **2011**, *6*, 101–107; b) Y. Chen, S. Song, Z. Yan, H. Fenniri, T. J. Webster, *Int. J. Nanomed.* **2011**, *6*, 1035–1044; c) Z. Huang, S.-K. Kang, M. Banno, T. Yamaguchi, D. Lee, C. Seok, E. Yashima, M. Lee, *Science* **2012**, *337*, 1521–1526.
[7] a) V. Vázquez-González, M. J. Mayoral, R. Chamorro, M. M. R. M. Hendrix, I. K. Voets, D. González-Rodríguez, *J. Am. Chem. Soc.* **2019**, *141*, 16432–16438; b) V. Vazquez-Gonzalez, M. J. Mayoral, F. Aparicio, P. Martinez-Arjona, D. Gonzalez-Rodriguez, *ChemPlusChem* **2021**, *86*, 1087–1096; c) M. González-Sánchez, M. J. Mayoral, V. Vázquez-González, M. Paloncýová, I. Sancho-Casado, F. Aparicio, A. de Juan, G. Longhi, P. Norman, M. Linares, D. González-Rodríguez, *J. Am. Chem. Soc.* **2023**, *145*, 17805–17818.
[8] a) F. Aparicio, P. B. Chamorro, R. Chamorro, S. Casado, D. González-Rodríguez, *Angew. Chem. Int. Ed.* **2020**, *59*, 17091–17096; b) P. B. Chamorro, F. Aparicio, R. Chamorro, N. Bilbao, S. Casado, D. González-Rodríguez, *Org. Chem. Front.* **2021**, *8*, 686–696.
[9] P. A. Korevaar, C. Schaefer, T. F. A. de Greef, E. W. Meijer, *J. Am. Chem. Soc.* **2012**, *134*, 13482–13491.
[10] a) S. Saeki, N. Kuwahara, M. Nakata, M. Kaneko, *Polymer* **1976**, *17*, 685–689; b) M. Naya, K. Kokado, K. B. Landenberger, S. Kanaoka, S. Aoshima, K. Sada, *Macromol. Chem. Phys.* **2020**, *221*, 1900455; c) G. D. Smith, D. Bedrov, *J. Phys. Chem. B* **2003**, *107*, 3095–3097; d) P. P. N. Syamala, F. Würthner, *Chem. Eur. J.* **2020**, *26*, 8426–8434; e) P. P. N. Syamala, B. Soberats, D. Görl, S. Gekle, F. Würthner, *Chem. Sci.* **2019**, *10*, 9358–9366; f) D. Görl, F. Würthner, *Angew. Chem. Int. Ed.* **2016**, *55*, 12094–12098.
[11] H. M. M. ten Eikelder, A. J. Markvoort, T. F. A. de Greef, P. A. J. Hilbers, *J. Phys. Chem. B* **2012**, *116*, 5291–5301.
[12] M. A. Beuwer, M. F. Knopper, L. Albertazzi, D. van der Zwaag, W. G. Ellenbroek, E. W. Meijer, M. W. J. Prins, P. Zijlstra, *Polym. Chem.* **2016**, *7*, 7260–7268.
[13] a) S. Prasad, K. Achazi, C. Bottcher, R. Haag, S. K. Sharma, *RSC Adv.* **2017**, *7*, 22121–22132; b) S. Guo, Y. Song, Y. He, X.-Y. Hu, L. Wang, *Angew. Chem. Int. Ed.* **2018**, *57*, 3163–3167; c) C. M. A. Leenders, L. Albertazzi, T. Mes, M. M. E. Koenigs, A. R. A. Palmans, E. W. Meijer, *Chem. Commun.* **2013**, *49*, 1963–1965; d) D. Janeliunas, R. Eelkema, B. Nieto-Ortega, F. J. Ramírez Aguilar, J. T. López Navarrete, L. van der Mee, M. C. A. Stuart, J. Casado, J. H. van Esch, *Org. Biomol. Chem.* **2013**, *11*, 8435–8442; e) M. Garzoni, M. B. Baker, C. M. A. Leenders, I. K. Voets, L. Albertazzi, A. R. A. Palmans, E. W. Meijer, G. M. Pavan, *J. Am. Chem. Soc.* **2016**, *138*, 13985–13995; f) M. H. Bakker, C. C. Lee, E. W. Meijer, P. Y. W. Dankers, L. Albertazzi, *ACS Nano* **2016**, *10*, 1845–1852.
[14] a) S. Pujals, N. Feiner-Gracia, P. Delcanale, I. Voets, L. Albertazzi, *Nat. Rev. Chem.* **2019**, *3*, 68–84; b) R. Jungmann, M. S. Avendaño, J. B. Woehrstein, M. Dai, W. M. Shih, P. Yin, *Nat. Methods* **2014**, *11*, 313–318.

Manuscript received: June 20, 2024
Accepted manuscript online: July 31, 2024
Version of record online: September 24, 2024